



Microstructure and Corrosion Behavior of the As-Extruded Mg–4Zn–2Gd–0.5Ca Alloy

Hao-Yi Niu¹ · Fang-Fang Cao¹ · Kun-Kun Deng¹ · Kai-Bo Nie¹ · Jin-Wen Kang¹ · Hong-Wei Wang¹

Received: 29 August 2019 / Revised: 11 October 2019 / Published online: 19 December 2019
© The Chinese Society for Metals (CSM) and Springer-Verlag GmbH Germany, part of Springer Nature 2019

Abstract

In order to study the corrosion resistance of extruded magnesium alloys, the Mg–4Zn–2Gd–0.5Ca alloy was extruded at the speed of 0.01–0.1 mm/s with the temperature of 280–360 °C in present study. Hot extrusion results show that the volume fraction of precipitates (V_{pre}), V_{DRX} (the dynamic recrystallization rate) and the average size of DRXed grain (d_{DRX}) decrease with the decrease in extrusion speed, and the corrosion rate of the alloy also shows a downward trend. On the contrary, the values of V_{pre} , V_{DRX} and d_{DRX} increase with the increase in extrusion temperature, and the corrosion resistance of Mg–4Zn–2Gd–0.5Ca alloy decreases. When the extrusion speed is 0.01 mm/s and the extrusion temperature is 280 °C, the alloy has the best corrosion resistance. The corrosion of extruded Mg–4Zn–2Gd–0.5Ca alloy occurs preferentially on the magnesium matrix around W and I phases in the DRXed zone. With the further corrosion, the corrosion continues to spread along the phase, and the corrosion area gradually increases. Galvanic corrosion plays a leading role in the corrosion process. Moreover, there are a large number of basal plane textures in the unDRXed region, which is conducive to improving the corrosion resistance of magnesium alloys. In addition, the decrease in grain size also makes the corrosion of magnesium alloy more uniform.

Keywords Mg–4Zn–2Gd–0.5Ca alloy · Extrusion · EIS (electrochemical impedance spectroscopy) · Weight loss · Corrosion resistance

1 Introduction

As structural and functional material, Mg and its alloy present many properties owing to its high specific strength, rigidity and good electromagnetic shielding properties. These performances make Mg alloy very attractive for applications in aerospace, automotive and electronic industries [1–4]. Moreover, due to the good biocompatibility and suitable degradation speed, Mg alloy also has a trend to replace traditional stainless steel as biomaterials [5, 6]. However, its application is limited because of the lower strength as well as the poor corrosion resistance [7–9]. Therefore, obtaining Mg alloy with high strength and corrosion performance has become a central issue in the current research filed.

The poor corrosion resistance of Mg alloy is mainly attributed to two aspects: (1) the lower electrochemical potential (–2.37 V vs SCE) and magnesium matrix often act as anode dissolved preferentially in the electrolyte; (2) the protective film is not as dense as the protective film of stainless steel and Al alloy [10–12]. Many efforts have been made to modify the anti-corrosion performance of Mg alloy, such as alloying and coating [13–18], of which the alloying can improve the corrosion resistance essentially [15], and the Mg–Zn–RE alloys have received the most concern [8, 19–21]. Among them, Yuan et al. [8] investigated the microstructure, mechanical properties and corrosion of Mg–2.4Zn–0.8Gd (wt%) alloy with and without solution treatment before extrusion in vitro. The research results show that the volume of secondary phases decreased after solution treatment, leading to more homogeneous microstructure distribution of as-extruded samples. The corrosion resistance was improved by about 20% according to hydrogen evolution and weight loss test. Zhang et al. [20] studied the microstructure, bio-corrosion behavior and cytotoxicity of an as-extruded Mg–11.3Gd–2.5Zn–0.7Zr (wt%) alloy. The results show

Available online at <http://link.springer.com/journal/40195>

✉ Kun-Kun Deng
jamsdk@163.com; dengkunkun@tyut.edu.cn

¹ Shanxi Key Laboratory of Advanced Magnesium-Based Materials, College of Materials Science and Engineering, Taiyuan University of Technology, Taiyuan 030024, China

that the microstructure of the as-extruded alloy mainly consists of the refinement grains. The corrosion rate in Hanks' solution is only 0.17 mm/year, and the corrosion mode of the alloy is uniform corrosion, which is much better than that of as-extruded Mg–10.2Gd–3.3Y–0.6Zr (wt%) alloy. There are long period stacking ordered (LPSO) phase, W phase ($\text{Mg}_3\text{Zn}_3\text{RE}_2$) and I phase ($\text{Mg}_3\text{Zn}_6\text{RE}$) formed when Zn/RE atomic ratio is different, which would influence its mechanical properties and corrosion resistance. As reported the corrosion resistance of $\text{Mg}_{95.5}\text{Gd}_{3.5}\text{Zn}_1$ with LPSO phase is better than that those without LPSO phase owing to the less accelerating corrosion process of LPSO phase [22], which was in agreement with Zhang's study [23]. Xu et al. [24] pointed out that the quasicrystal I phase has a series of advantages, such as high hardness, low interfacial energy, outstanding corrosion resistance, etc. Although the strength of rare earth Y containing Mg–Zn–RE alloys was enhanced with the increase in I phase [25], the corrosion mechanism of I phase on Mg–Zn–RE alloy is not clear.

Besides, studies have displayed that the addition of Ca had an important influence on the microstructure of Mg alloys by refining grain size and scattering the particles to lead to a more uniformed distribution which can further affect the corrosion behavior and mechanical properties [26–28]. Zeng et al. [26] analyzed the microstructure, composition and the corrosion resistance of Mg–Ca alloys. The results revealed that Ca played a dual role, decreasing the corrosion rate due to the refinement of grain size and accelerating corrosion due to the formation of the Mg_2Ca phase. The Mg_2Ca particles coexisted with Fe and Si leading to pitting corrosion.

Thermodynamic deformation (hot rolling, extrusion, etc.) has been reported to enhance the mechanical properties and corrosion resistance of Mg alloy [11, 29–31]. Li et al. [31] pointed out that excellent mechanical properties could be achieved with the YS of 324 MPa and UTS of 371 MPa for Mg–4Zn–0.5Ca alloy extruded at 0.01 mm/s. Furthermore, the type, amount and distribution of phase also changed during deformation process which affects the corrosion resistance. Wu et al. [11] reported that the corrosion properties of Mg–Al–Ca alloys was improved after extrusion due to the broken of $(\text{Mg}, \text{Al})_2\text{Ca}$ or Al_2Ca and grain refinement. Cao et al. [30] pointed out that the corrosion resistance of Mg–Gd, Mg–Ca and Mg–Al alloys could be improved after hot rolling due to the more homogeneous microstructure as well as the less, smaller secondary phase. At present, there are few reports about the corrosion performance of Mg–Zn–Ca alloy with rare earth element. Herein, the corrosion behavior of Mg–4Zn–0.5Ca alloy containing Gd under different extrusion speeds and temperatures was studied and discussed in this study.

2 Experimental

2.1 Material Preparation

Mg–4Zn–2Gd–0.5Ca (wt%) alloy was prepared by traditional casting method with an resistance furnace melting of high-purity Mg (99.95%), Zn (99.95%), Ca (99.95%) and Mg–30Gd master alloy under a shielding gas of CO_2 and SF_6 , of which the volume ration is 40:1, and then, they were cast into a mold with a diameter of 41 mm preheated to 250 °C. After that, two steps of homogenization treatment were applied: firstly, the ingot was homogenized at 430 °C for 16 h, and then, it was treated at the temperature to 510 °C for 20 h. The ingot for extrusion was machined with a diameter of 40 mm and a length of 45 mm. For different extrusion speeds, the ingots were extruded at 280 °C with speed of 0.01, 0.05 and 0.1 mm/s, respectively. And the ingots were denoted as 280–0.01, 280–0.05 and 280–0.1, respectively. For different temperatures of extrusion, the ingots were extruded at 0.01 mm/s with temperature of 320 and 360 °C, respectively. And the ingots were denoted as 320–0.01 and 360–0.01, respectively. The extrusion ratio of all extruded specimens was 16:1. Finally, the rods of 10 mm in diameter were obtained. The corresponding experimental device in this study is shown in Fig. 1.

2.2 Microstructure Observation

The actual chemical compositions of Mg–4Zn–2Gd–0.5Ca alloy are listed in Table 1. The specimens for microstructure observation were machined parallel to the direction of extrusion and then ground, polished and etched. OM (optical microscopy, 4XC) and scanning electron microscopy (SEM) were used to observe the microstructure as well as the corrosion morphology. The average size (d_{DRX}) and volume fraction (V_{DRX}) of dynamic recrystallization grains and precipitates were measured using Image-Pro Plus 6.0 (Media Cybernetics, Bethesda, Maryland). The chemical composition of the phase was determined by XRD (X-ray diffractometer, DX-2700), SEM with EDS (energy-dispersive spectrometer) and TEM (transmission electron microscopy, JEM-2100) combined with EDS. The scanning range of XRD was 20°–80°, and the scan rate was 2°/min. The obtained results were analyzed using MDI Jade 6.0 software. TEM sample was ground to below 50 μm firstly, and then, it underwent ion-thinning with an ion accelerating voltage of 200 kV.

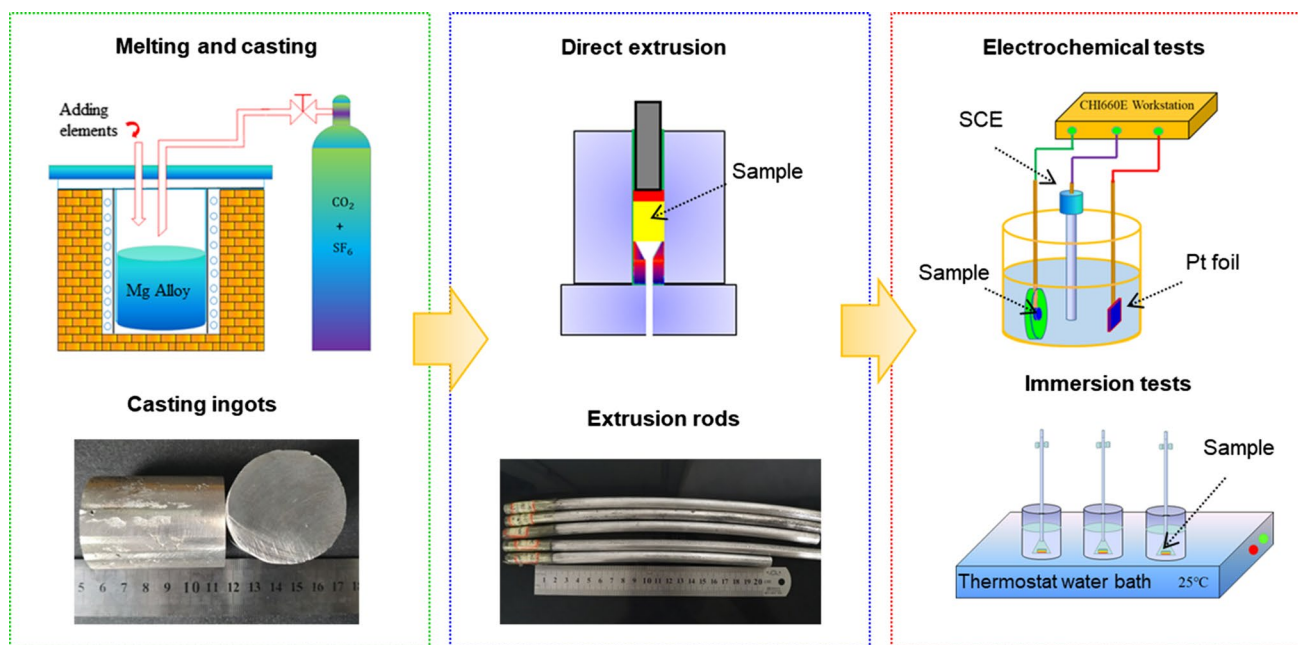


Fig. 1 Schematic for the experimental device in this study

Table 1 Actual chemical compositions of Mg–4Zn–2Gd–0.5Ca alloy (wt%)

Zn	Gd	Ca	Mg
4.2	2.1	0.3	Balance

2.3 Electrochemical Tests

Electrochemical tests were carried on at 25 ± 1 °C using a three-electrode system with a saturated calomel electrode (SCE) acting as reference electrode, a platinum electrode acting as counter electrode and the specimen acting as working electrode. Before tests, the working electrode was connected to a copper wire and sealed up with epoxy resin leaving an uncovered surface of 10 mm in diameter, and then it was ground, polished, washed and dried. Prepared specimens were soaked in 3.5 wt% NaCl solution for 0.5 h to get a steady open circuit potential (OCP, V vs SCE). After that, electrochemical impedance spectroscopy (EIS) measurements were accomplished within a frequency range of 100 k Hz–0.01 Hz accompanied by the amplitude of 5 mV. The corresponding EIS information and fitted curves were obtained by ZSimpwin. Prior to potentiodynamic polarization test, the samples were immersed in 3.5 wt% NaCl solution for 60 min; polarization tests were conducted with a scan rate of 0.5 mV s^{-1} from -1.9 to -1.3 V.

2.4 Immersion Tests

The as-extruded Mg–4Zn–2Gd–0.5Ca alloys were immersed in 3.5 wt% NaCl solution and sustained for 148 h at 25 ± 1 °C. The specimens for immersion test were machined parallel to the direction of extrusion with a 5 mm radius and 5 mm thickness and sealed with epoxy resin and then ground to 4000#, polished and weighted. Hydrogen evolution and weight loss experiments were performed simultaneously. An inverted funnel and an acid burette were placed above the specimen soaked in the beaker to record the produced hydrogen volume and recorded every 4 h; then, the hydrogen evolution rate [HER, $\text{ml}/(\text{cm}^2 \cdot \text{h})$] was calculated. After immersion, the corrosion products formed on the surface were washed away using 200 g/L CrO_3 + 10 g/L AgNO_3 , and then, the specimens were dried and weighted again. The weight loss Δm can be translated into corrosion rate C_w (mm/year) using the following formula [11]:

$$C_w = \frac{2.1\Delta m}{At}, \quad (1)$$

here C_w was the corrosion rate (mm/year); Δm was the weight loss (mg); A was the exposed area of the specimens (cm^2); t was the immersion time (day).

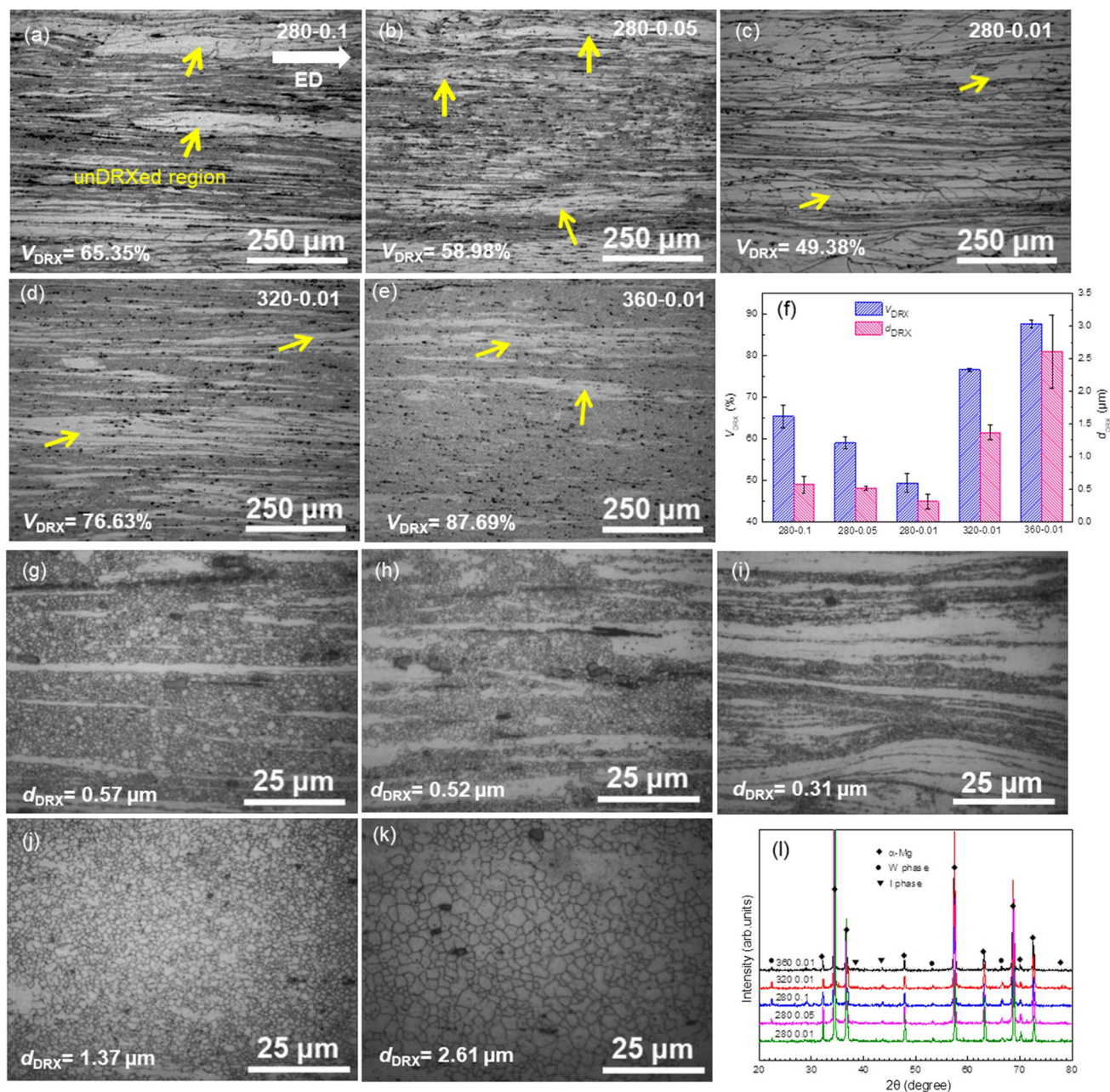


Fig. 2 OM of as-extruded Mg–4Zn–2Gd–0.5Ca alloy: **a, g** 280 °C, 0.1 mm/s, **b, h** 280 °C, 0.05 mm/s, **c, i** 280 °C, 0.01 mm/s, **d, j** 320 °C, 0.01 mm/s, **e, k** 360 °C, 0.01 mm/s, **f** V_{DRX} and d_{DRX} of the Mg–4Zn–2Gd–0.5Ca alloy, **l** XRD pattern of as-extruded Mg–4Zn–2Gd–0.5Ca alloy

3 Results

3.1 Microstructures of As-Extruded Mg–4Zn–2Gd–0.5Ca Alloy

Figure 2 depicts the OM, the DRXed rate and the DRXed grain size of as-extruded Mg–4Zn–2Gd–0.5Ca alloy parallel to extrusion direction (ED) at different extrusion speeds and temperatures. It can be obviously seen that the as-extruded alloy consists of unDRXed area with strip distribution along

the extrusion direction and DRXed regions with fine grains in the low magnification map of Fig. 2a–e. The d_{DRX} is only 0.31 μm when extruded at 0.01 mm/s, 280 °C; however, V_{DRX} is only 49.4%. The V_{DRX} and d_{DRX} increase gradually and the strip distribution in unDRXed area decreases with increasing the extrusion speed and temperature.

The XRD results (Fig. 2l) show that the as-extruded alloy consists of α -Mg, W phase ($Mg_3Zn_3Gd_2$) and I phase (Mg_3Zn_6Gd). The SEM morphology of as-extruded Mg–4Zn–2Gd–0.5Ca alloy parallel to the extrusion direction

at different extrusion speeds and temperatures is presented in Fig. 3. Distinctly to observed in Fig. 3a, c, e, g, i, the secondary phase distributed in strips along extrusion direction and the EDS results (Table 2) display the secondary phase containing Mg, Zn and Gd; the Zn/Gd ratio is about 3:2 which is close to W phase. Combining with the XRD analysis, it can be determined that the secondary phase is W phase. Besides that, the spherical precipitate distributed within the grain boundaries and at grain interiors of the DRXed region can be seen at the high magnification in Fig. 3b, d, f, h, j. Figure 4 presents the TEM result of the as-extruded 360–0.01 alloy, and the spherical precipitate can also be seen in Fig. 4a. The EDS analysis for the precipitate marked by arrow in Fig. 4b shows that the main elements contain Mg, Zn and Gd; the Zn/Gd ratio is about 6 which is close to I phase. Combining with the XRD analysis, it can be determined that the spherical precipitate is I phase. It is worth noting that the V_{pre} of I phase increases with increasing extrusion speed and temperature.

3.2 Electrochemical Measurements

Figure 5 shows the OCP curve of as-extruded Mg–4Zn–2Gd–0.5Ca alloy immersed in 3.5 wt% NaCl solution for 0.5 h. The OCP of all the alloys increases drastically in the first 200 s and then grows a little bit obtaining a relatively stable value after immersion for about 30 min. Generally speaking, the increase in the OCP potential value indicates the formation of the corrosion layer over the time [32]; the more positive value means the higher fraction corrosion layer formed [33]. But only OCP value is not sufficient to explain the corrosion resistance of the alloy.

Figure 6 displays the EIS diagrams of Nyquist and Bode plots. The Nyquist plot (Fig. 6a) consisted of three well-defined flat semicircle loops, and the diameters are different indicating the same corrosion mechanism, but different corrosion rates. The three loops correspond to the high-frequency capacitive loop, middle-frequency capacitive loop and low-frequency inductive loop, respectively, which is relative to the wave crest and wave trough (Fig. 6c). Ordinarily speaking, the high-frequency capacitive loop represents the charge transfer process and the specimens begin to deteriorate; the middle-frequency capacitive loop attributed to the generation and diffusion of porous film of the alloy, and the porous film is probably Mg(OH)₂ [34, 35]; the inductive loop indicates the Cl[−] penetrates the porous film and infiltrate the substrate.

As for the Mg–4Zn–2Gd–0.5Ca alloy extruded at 280 °C with different speeds, the diameter of the semicircle loops decreases with increasing the extrusion rate, which is related to the worse corrosion performance of the alloy. The Bode plots (Fig. 6b) of extrusion alloy at 0.01 mm/s are higher than others, which are corresponding well with the Nyquist

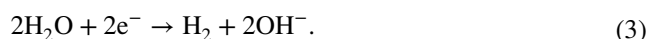
plots. As for the specimen extruded at different temperatures, the corrosion resistance is the best when the extrusion temperature is 280 °C. And the corrosion resistance of the alloy decreases with the increase in the extrusion temperature, and the difference of corrosion resistance for the alloy extruded at 320 °C and 360 °C is negligible.

To better elucidate the corrosion feature of as-extruded Mg–4Zn–2Gd–0.5Ca alloy, the fitted circuit model is shown in Fig. 6d. Where R_s , R_{ct} , R_f and R_L stand for the solution resistance, charge transfer resistance, film resistance and induction resistance, respectively. CPE represents the constant phase element that replaces the electric double-layer capacitor, and L represents the inductance. The relevant electrochemical data are listed in Table 3. Where R_{ct} is a measure of the corrosion rate, and its value is inversely proportional to corrosion rate [34]; it is noted that the value of R_{ct} for the specimen extruded with 0.01 mm/s at 280 °C reached up 1278 Ω cm² which is the largest of the alloy; that is to say, the specimen for 280–0.01 has the optimal corrosion resistance, which becomes worse with increasing extrusion rate and temperature.

The potentiodynamic polarization curves of as-extruded Mg–4Zn–2Gd–0.5Ca alloy immersed in 3.5 wt% NaCl for 1 h are depicted in Fig. 7a. Due to negative difference effect (NDE), values of corrosion current density (i_{corr}) are obtained by cathode extrapolation. The corrosion potential (E_{corr}) and corrosion current density (i_{corr}) are presented in Table 4. Generally, the anodic part mainly produces the following reaction:



The cathode region of the polarization curve mainly produces the following reaction:



In case of the alloy at different extrusion speeds, the difference of the E_{corr} is very small indicating that the alloys extruded at different conditions have similar thermodynamic characteristic. However, obvious shift to right of cathode branch is observed indicating the value of i_{corr} increases with increasing extrusion rate; the alloy with the rate of 0.1 mm/s at 280 °C exhibits the highest i_{corr} of 20.90 μA/cm², which is about three times higher than that in 0.01 mm/s at 280 °C, suggesting that the 280–0.1 alloy has a poor corrosion resistance. Song et al. [33] revealed that i_{corr} is more precise in explaining the corrosion resistance than the E_{corr} . The E_{corr} merely represent the thermodynamic characteristic rather than the corrosion kinetics. Similarly, in case of the alloy at different extrusion temperatures, the thermodynamic characteristic is similar and the i_{corr} increases slightly with increasing extrusion temperature. It is worth noting that all the

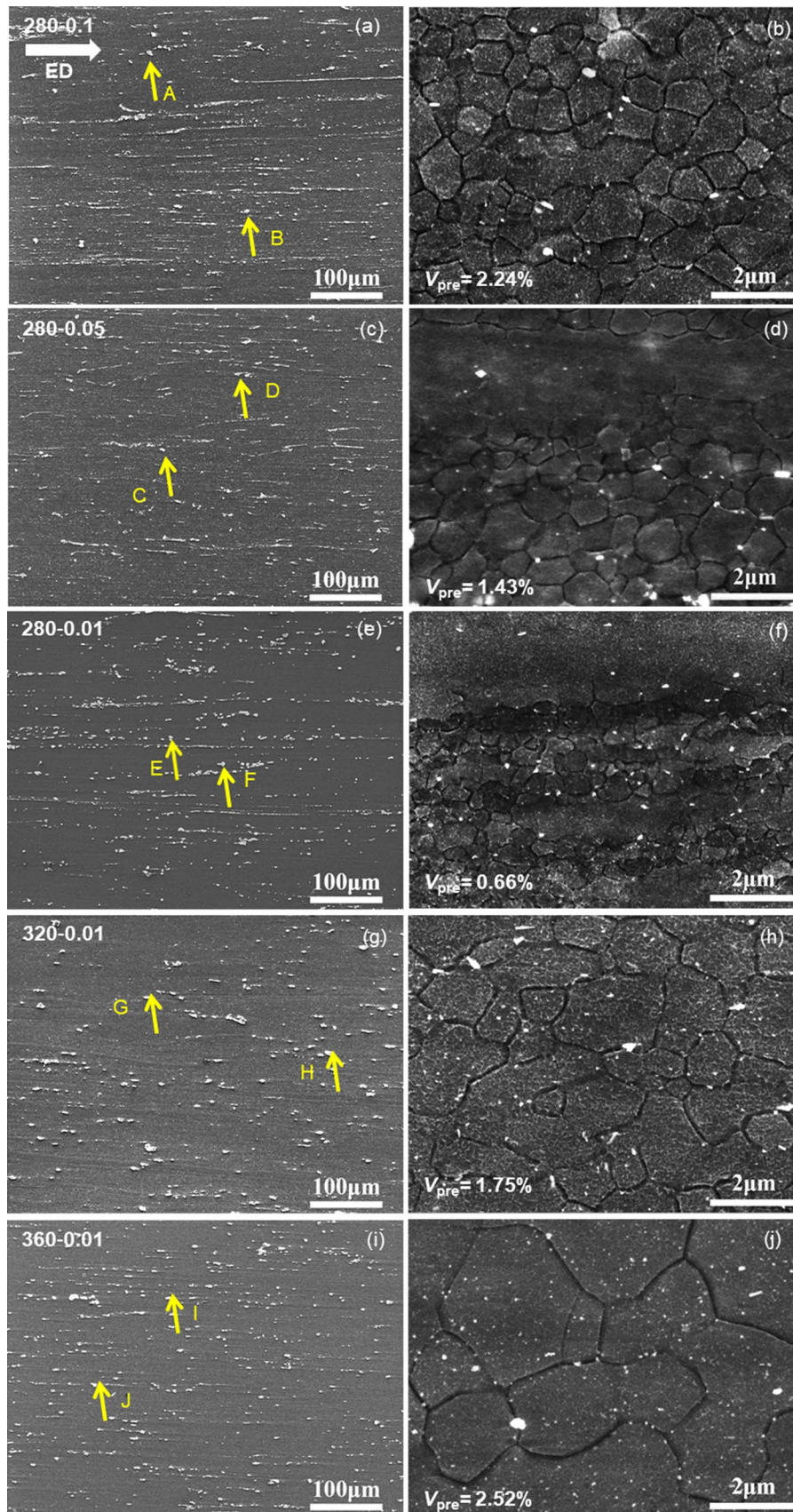


Fig. 3 SEM microstructures of as-extruded Mg–4Zn–2Gd–0.5Ca alloy: **a, b** 280 °C, 0.1 mm/s, **c, d** 280 °C, 0.05 mm/s, **e, f** 280 °C, 0.01 mm/s, **g, h** 320 °C, 0.01 mm/s, **i, j** 360 °C, 0.01 mm/s

alloys show an inflection point at the anode branch, which indicates that the surface film is generated on the alloy. When the potential reaches the film breakdown potential, the protective film starts to break up and pitting corrosion occurs [36]. Overall, the alloy with extrusion temperature of 280 °C at 0.01 mm/s has the best corrosion resistance, and the corrosion resistance of specimen extruded at 320 °C is not far different from that of the specimen extruded at 360 °C.

Table 2 EDS analysis results of as-extruded Mg–4Zn–2Gd–0.5Ca alloy (at.%)

Positions	Elements				Possible compounds
	Mg	Zn	Gd	Ca	
A	42.7	35.0	22.2	0.0	W phase (Mg ₃ Zn ₃ Gd ₂)
B	27.0	54.8	18.2	0.0	W phase (Mg ₃ Zn ₃ Gd ₂)
C	52.6	27.0	20.2	0.1	W phase (Mg ₃ Zn ₃ Gd ₂)
D	24.8	55.7	19.5	0.0	W phase (Mg ₃ Zn ₃ Gd ₂)
E	25.3	54.0	20.2	0.0	W phase (Mg ₃ Zn ₃ Gd ₂)
F	25.5	52.2	22.3	0.0	W phase (Mg ₃ Zn ₃ Gd ₂)
G	27.6	53.9	18.4	0.0	W phase (Mg ₃ Zn ₃ Gd ₂)
H	27.9	53.1	19.0	0.0	W phase (Mg ₃ Zn ₃ Gd ₂)
I	29.5	51.5	18.2	0.8	W phase (Mg ₃ Zn ₃ Gd ₂)
J	29.6	50.5	19.9	0.0	W phase (Mg ₃ Zn ₃ Gd ₂)

The polarization resistance, R_p , is a parameter that characterizes corrosion and its reciprocal varies directly as the corrosion rate. R_p was calculated by the equivalent circuit from the following formula:

$$R_p = R_s + \frac{R_{ct}(R_f + R_L)}{R_{ct} + R_f + R_L} \quad (4)$$

And the $1/R_p$ of the Mg–4Zn–2Gd–0.5Ca alloy immersed in 3.5 wt% NaCl for 40 min is depicted in Fig. 7b. The 280–0.01 alloy presents the lowest value level of $1/R_p$ than others. To put it differently, the corrosion rate decreased with decreasing extrusion speed and extrusion temperature.

3.3 Immersion Measurements

In order to determine the results obtained by electrochemical measurements, the weight loss and hydrogen evolution tests were conducted, respectively. Figure 8a, b presents the HER and C_w calculated by immersion measurements by immersing in 3.5 wt% NaCl solution for 148 h, respectively. The general trend is coinciding with those obtained by potentiodynamic polarization and electrochemical impedance tests. The corrosion rate of the 280–0.01 alloy is the lowest with 7.4 mm/year, showing up the best corrosion resistance. It has been shown that the HER is relatively stable at the first 60 h and then improves greatly, which indicates that porous film generated on the surface is destroyed and chloride ion penetrates the porous film into the substrate and induces the corrosion degree to be aggravated.

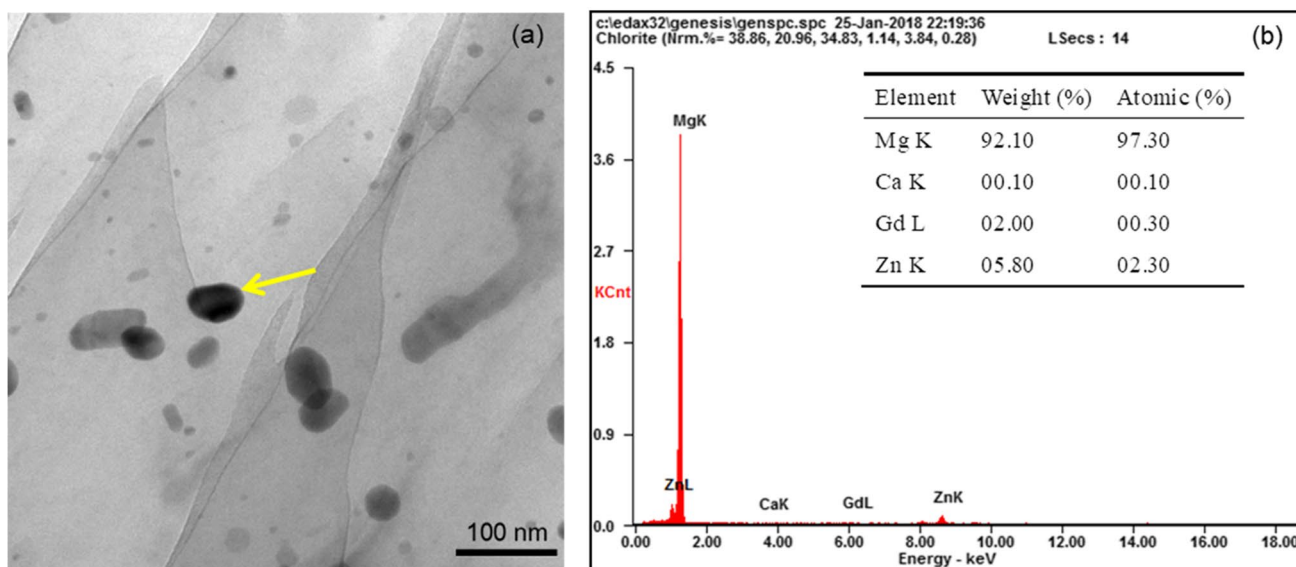


Fig. 4 TEM image of as-extruded 360 °C 0.01 mm/s Mg–4Zn–2Gd–0.5Ca alloy, and **b** the corresponding EDS of the precipitate pointed by the yellow arrow in **a**

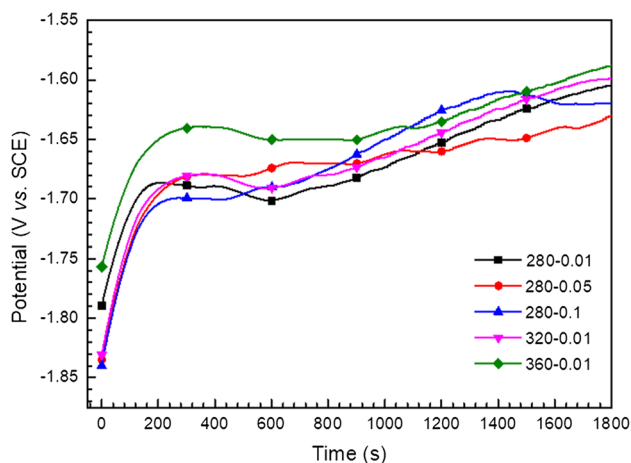


Fig. 5 OCP curves of as-extruded Mg-4Zn-2Gd-0.5Ca alloy immersed in 3.5 wt% NaCl solution for 30 min

3.4 Cross-Sectional Corrosion Morphology

The cross-sectional images of extruded Mg-4Zn-2Gd-0.5Ca alloys immersed in 3.5 wt% NaCl for 148 h removing the corrosion product are given in Fig. 9. Through long-term immersion, the result shows that the overall corrosion of the 280-0.01 alloy is the shallowest. The corrosion is more serious with increasing extrusion speed and temperature, and the corrosion surface of the 280-0.1 alloy is the most uneven, which is consistent with the results obtained from the EIS, polarization and immersion tests.

4 Discussion

According to above electrochemical measurements and immersion tests, the as-extruded 280-0.01 alloy demonstrates the best corrosion resistance, and the corrosion resistance deteriorates with increasing extrusion speed

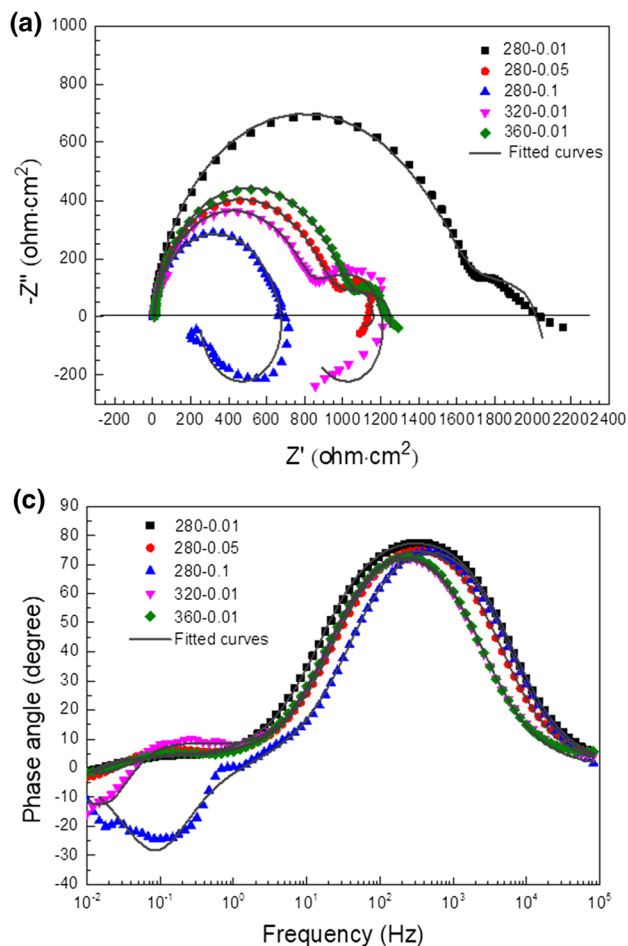


Fig. 6 EIS of as-extruded Mg-4Zn-2Gd-0.5Ca alloy immersed in 3.5 wt% NaCl solution for 40 min. **a** Nyquist diagrams, **b** Bode plots of frequency versus Z and **c** Bode plots of frequency versus phase angle, **d** equivalent circuit of as-extruded Mg-4Zn-2Gd-0.5Ca alloy. Where the R_s represents the solution resistance; CPE represents the constant phase element; R_{ct} represents the charge transfer resistance; R_f represents the film resistance; L represents the inductance; and R_L represents the induction resistance

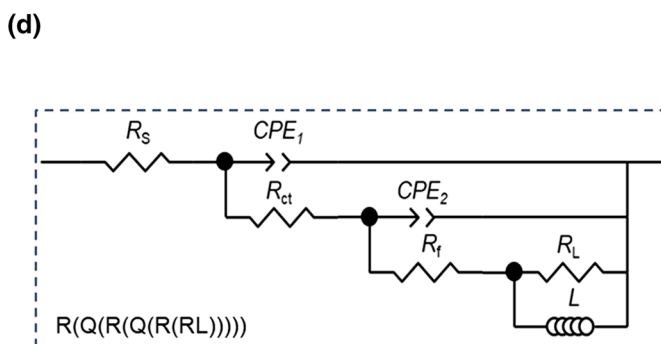
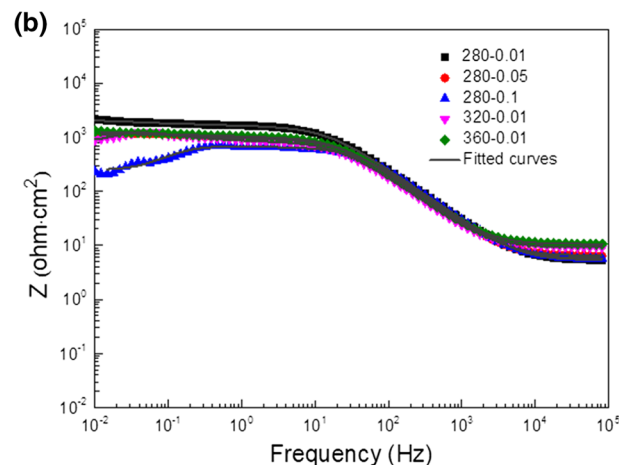
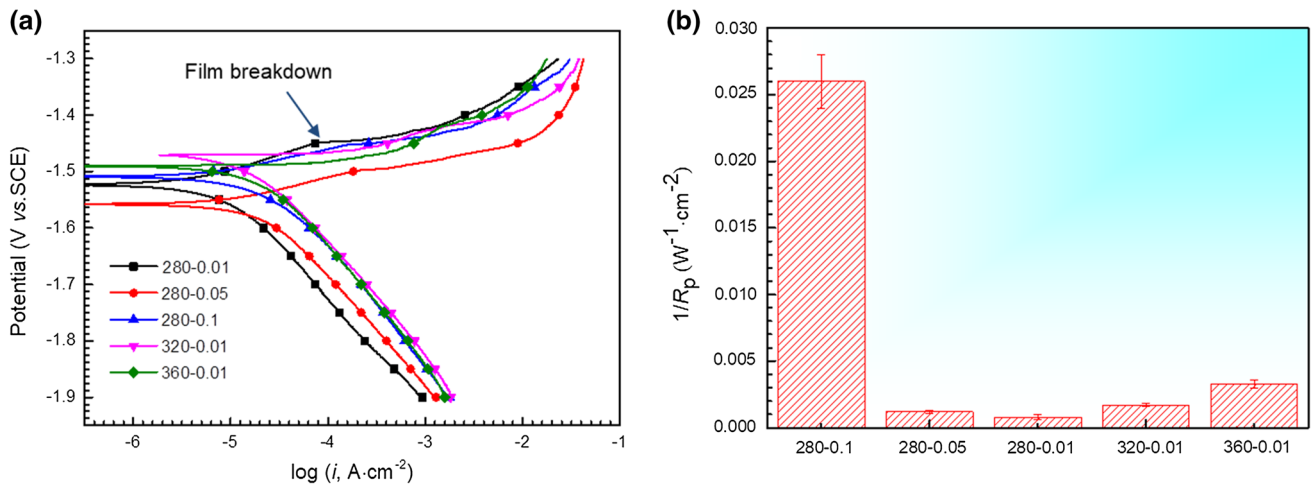


Table 3 EIS data parameters obtained from EIS analysis of as-extruded Mg–4Zn–2Gd–0.5Ca alloy immersed in 3.5 wt% NaCl solution for 40 min

Materials	R_s (Ω)	CPE_1 ($10^{-6} s^n \Omega^{-1} cm^{-2}$)	n_1	R_{ct} (Ωcm^2)	CPE_2 (10^{-5} $s^n \Omega^{-1} cm^{-2}$)	n_2	R_f (Ωcm^2)	R_L (Ωcm^2)	$L(H)$
280–0.1	5.745	8.49	0.948	33.9	7.9	0.22	225.2	490.6	541.7
280–0.05	6.476	10.63	0.937	823.7	411.9	0.24	382.4	6.87×10^{10}	4.63×10^3
280–0.01	5.346	9.47	0.935	1278	197.1	0.14	292	4.41×10^9	3.78×10^4
320–0.01	9.316	13.77	0.929	803.9	261.3	0.63	1464	538.6	3086
360–0.01	10.54	11.61	0.935	954.1	361.7	0.43	0.01	413.8	1.26×10^4

**Fig. 7** a Potentiodynamic polarization curves and b $1/R_p$ of as-extruded Mg–4Zn–2Gd–0.5Ca alloy immersed in 3.5 wt% NaCl solution for 1 h**Table 4** Corrosion potential (E_{corr}), cathodic slope (β_c) and corrosion current density (i_{corr}) obtained from polarization curves of as-extruded Mg–4Zn–2Gd–0.5Ca alloy immersed in 3.5 wt% NaCl solution for 1 h

Materials	E_{corr} (V vsSCE)	β_c (mv/dec)	i_{corr} ($\mu A/cm^2$)
280–0.1	–1.546	-151.31 ± 38.47	20.90 ± 9.51
280–0.05	–1.557	-129.12 ± 1.24	11.40 ± 2.83
280–0.01	–1.522	-121.34 ± 3.77	6.35 ± 2.14
320–0.01	–1.469	-118.99 ± 1.27	8.42 ± 0.28
360–0.01	–1.489	-112.02 ± 11.33	7.55 ± 4.04

and extrusion temperature. Generally speaking, corrosion behavior of magnesium alloy strongly depends on its microstructure, such as grain size, the type and quantity of secondary phase, texture, etc. Consequently, Fig. 10 describes the curves of corrosion rate of Mg–4Zn–2Gd–0.5Ca alloy under different extrusion conditions with V_{pre} , V_{DRX} and d_{DRX} . It can be seen that the corrosion resistance of the alloy increases with the decrease in extrusion rate at 280 °C. However, the V_{pre} , V_{DRX} and d_{DRX} show a downward trend. This is mainly attributed to the reduction of precipitates,

which reduces the chance of galvanic corrosion between the matrix and the precipitates. Besides, the decrease in V_{DRX} and d_{DRX} can help to reduce the corrosion rate of the Mg–4Zn–2Gd–0.5Ca alloy. Furthermore, when the extrusion rate is 0.01 mm/s, with increase in extrusion temperature, the V_{pre} , V_{DRX} and d_{DRX} in the matrix increase, and the corrosion resistance of the alloy decreases. In other words, the alloy has the optimum corrosion resistance when the values of the V_{pre} , V_{DRX} and d_{DRX} in the matrix are all low. In addition, compared with the results of Cao et al. [37], the corrosion resistance of Mg–4Zn–2Gd–0.5Ca alloy (7.4 mm/year) extruded at 280 °C–0.01 mm/s is obviously improved than that of Mg–4Zn–2Gd–0.5Ca alloy treated by 6 passes of MDF (10.6 mm/year). At the same time, the corrosion resistance of Mg–4Zn–2Gd–0.5Ca alloy (7.4 mm/year) extruded at 280 °C–0.01 mm/s increased by 57.23%, compared with that of Mg–15.24Gd–4.75Zn alloy (17.3 mm/year) treated with T4 [38].

To announce the corrosion feature of Mg–4Zn–2Gd–0.5Ca alloy, its surface morphology is immersed in 3.5 wt% NaCl for 40 min removing the corrosion product as given in Fig. 11. After short time immersion, the mechanism of corrosion under different extrusion

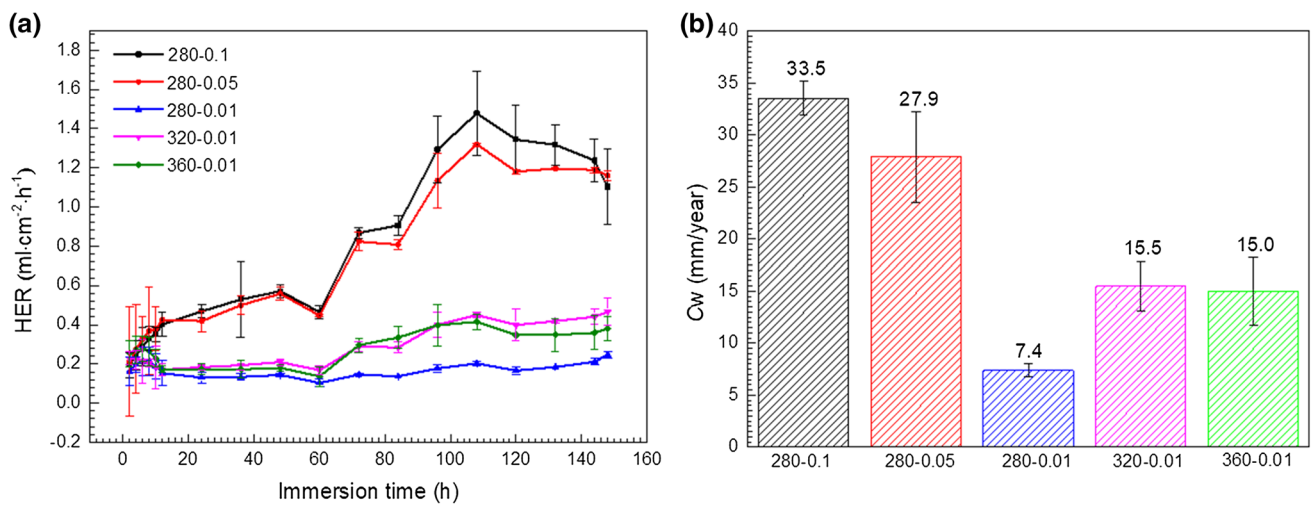


Fig. 8 Immersion test result **a** hydrogen evolution rate plot and **b** weight loss of as-extruded Mg–4Zn–2Gd–0.5Ca alloy immersed in 3.5 wt% NaCl solution for 148 h

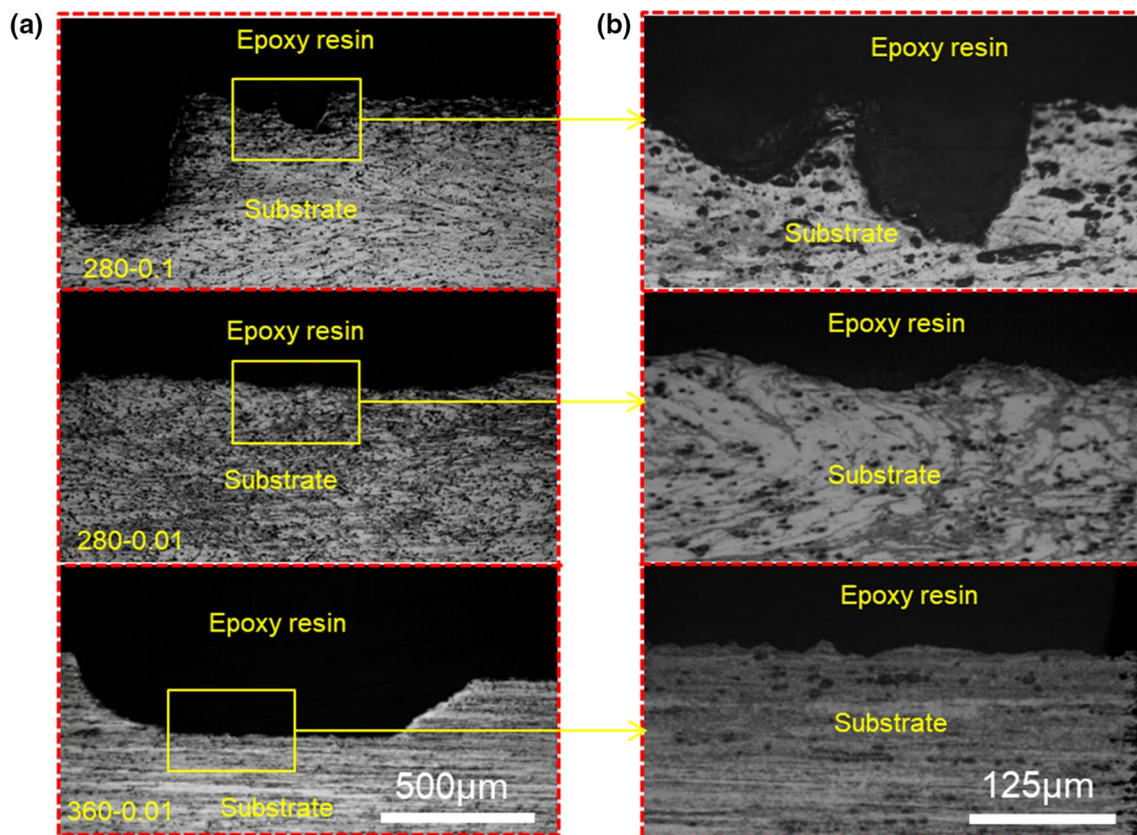


Fig. 9 Section corrosion morphology of as-extruded Mg–4Zn–2Gd–0.5Ca alloy immersed in 3.5 wt% NaCl solution for 148 h: **a** low magnification; **b** high magnification

parameters is the same, all of which showing two kinds of corrosion morphology. Some show the uniform corrosion morphology, as shown by the yellow arrows in Fig. 11a, d,

g. The other corrosion morphology is galvanic corrosion, as depicted in Fig. 11b, e, h. Abundant shallow corrosion pits on the surface and on corroded α -Mg substrate around the

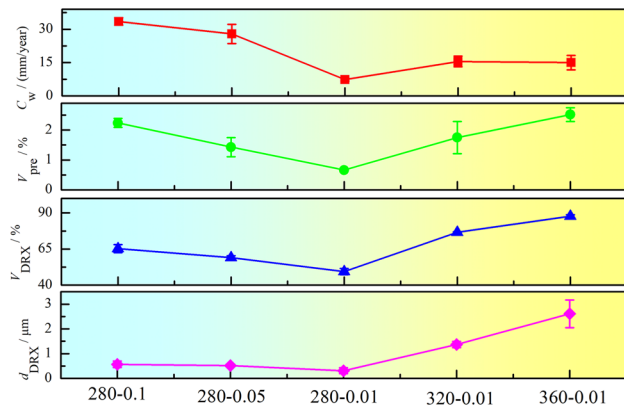


Fig. 10 Curves of corrosion rate of Mg–4Zn–2Gd–0.5Ca alloy under different extrusion conditions with V_{pre} , V_{DRX} and d_{DRX}

phase in high magnification map of Fig. 11c, f, i are shown by yellow arrows and white arrows, respectively. This may be caused by the stringer-shape dispersed W phase and precipitated I phase.

During the period of corrosion, the standard electrode potential of W phase and I phase is higher than α -Mg

substrate [21] and the site where the potential is lower acts as anode with respect to the higher potential; galvanic couple generates between the phase and α -Mg substrate, and substrate is preferentially corroded as the anode. Corrosion continually propagates along the horizontal direction, and the phase will fall off when the surrounding α -Mg substrate is sufficiently dissolved, leading to the formation of circular corrosion pits.

Nevertheless, it should be noted that the degree of DRX strongly depends on extrusion conditions. The DRX is incompletely in present extrusion conditions, the microstructure of which contains both the unDRXed regions and DRXed regions, as described in Fig. 2. As compared with the DRXed regions, the basal plane texture is much stronger in the unDRXed regions [39]. It has been verified that the Mg alloys with strong basal plane texture usually possess the lower corrosion rate for the reason that the basal plane owns stronger atomic bonding and higher atomic coordination [40]. On the contrary, the W phase and I phase are mainly distributed in the DRXed region and the corrosion occurred preferentially at this place. Besides, the precipitated I phase in unDRXed regions is far less than that in the DRXed regions. That means the

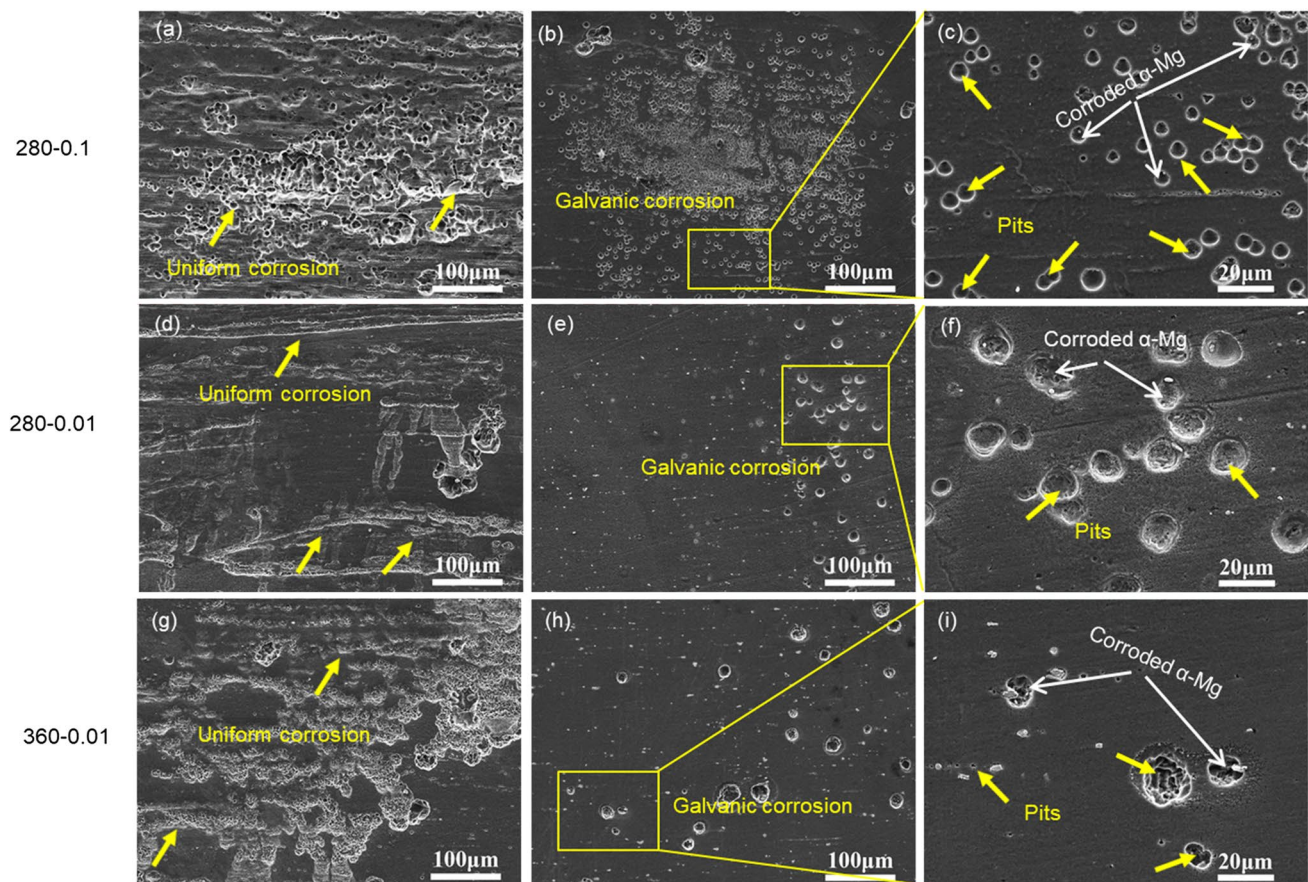


Fig. 11 Corrosion morphologies of as-extruded Mg–4Zn–2Gd–0.5Ca alloy immersed in 3.5 wt% NaCl solution for 40 min: **a–c** 280 °C, 0.1 mm/s; **d–f** 280 °C, 0.01 mm/s; **g–i** 360 °C, 0.01 mm/s

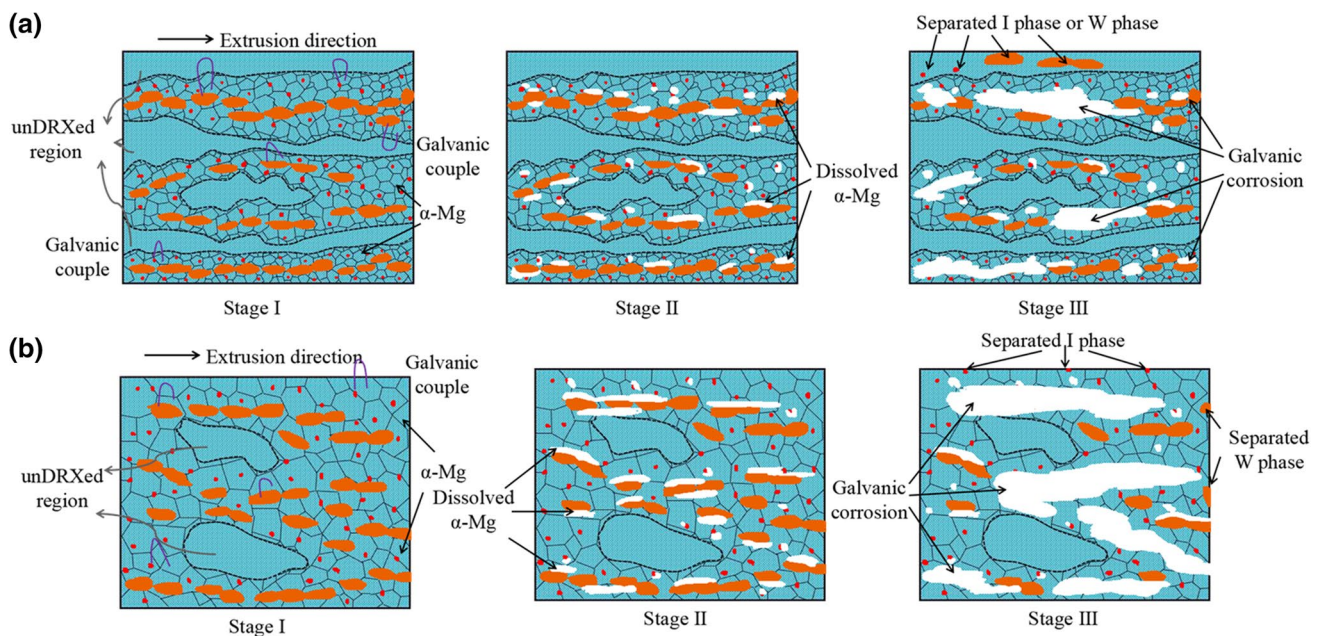


Fig. 12 Schematic illustrations of corrosion mechanism for the as-extruded Mg–4Zn–2Gd–0.5Ca alloy: **a** less DRXed region; **b** more DRXed region

unDRXed regions may have much more Gd content than the DRXed regions. According to Ref [41], the dissolution of rare earth elements can form a more stable protective film, which increases the difficulty of corrosion reaction to some extent and increases the corrosion resistance. Owing to above reasons, the corrosion resistance of unDRX regions is better than that of the DRXed region in present Mg–4Zn–2Gd–0.5Ca alloy.

To better reveal corrosion behavior about the as-extruded Mg–4Zn–2Gd–0.5Ca alloy, the schematic illustration is presented in Fig. 12. The corrosion mechanism concerning Mg–4Zn–2Gd–0.5Ca alloy containing a large amount of unDRXed regions is presented in Fig. 12a. In Stage I, the W and I phases are distributed in DRXed region, wherein the W phase is striped along the extrusion direction. The corrosion preferentially occurs in the DRXed region, and the galvanic couples are formed between phase and α -Mg substrate. In stage II, the potential of α -Mg substrate is lower than the phase, and the substrate acts as anode and the phase is cathode; galvanic corrosion occurs, and α -Mg near the phase dissolves preferentially, as revealed by the black arrows. In stage III, more and more Cl^- penetrates into the substrate and corrosion continues to propagate around the phase, and the area of corrosion increases gradually, resulting in the falling off of the W and I phases.

Accompanied with increasing extrusion rate and temperature, the degree of DRX in Mg–4Zn–2Gd–0.5Ca alloy increases obviously, and the corrosion behavior containing a large amount of DRXed regions is described in Fig. 12b.

Due to the existence of a great deal of precipitate, galvanic corrosion acts a dominant part in the procedure of corrosion.

5 Conclusions

1. With the decrease in extrusion speed, the V_{pre} , V_{DRX} and d_{DRX} of Mg–4Zn–2Gd–0.5Ca alloy decrease, and the corrosion rate also decreases. With the increase in extrusion temperature, the values of V_{pre} , V_{DRX} and d_{DRX} increase, and the corrosion resistance of the alloy decreases.
2. When the extrusion rate is 0.01 mm/s and the extrusion temperature is 280 °C, the alloy has the best corrosion resistance, and the corrosion rate is 7.37 mm/year.
3. The main factors affecting the extruded Mg–4Zn–2Gd–0.5Ca alloy are V_{pre} , V_{DRX} and d_{DRX} . The lower precipitated phase reduces the chance of galvanic corrosion between matrix and precipitated phase. Moreover, the decrease in V_{DRX} and d_{DRX} increases the basal texture of the alloy surface, which makes the corrosion slow and uniform.
4. The corrosion of extruded Mg–4Zn–2Gd–0.5Ca alloy occurs preferentially on the magnesium matrix around W and I phases in the DRXed zone. With the further corrosion, the corrosion continues to spread along the phase, and the corrosion area gradually increases. Galvanic corrosion plays a leading role in the corrosion process.

Acknowledgements This work was financially supported by the National Natural Science Foundation of China (Nos. 51771128, 51771129 and 51201112), the Projects of International Cooperation in Shanxi (No. 201703D421039) and the Natural Science Foundation of Shanxi (No. 201601D011034).

References

- [1] Q.X. Shi, C.J. Wang, K.K. Deng, K.B. Nie, M. Cao, W.M. Gan, W. Liang. *Mater. Sci. Eng. A*. **772**, 138827 (2020)
- [2] B.J. Wang, D.K. Xu, J. Sun, E.H. Han, *Corros. Sci.* **157**, 347 (2019)
- [3] P.P. Wu, K.K. Deng, K.B. Nie, Z.Z. Zhang, *Acta Metall. Sin. (Engl. Lett.)* **32**, 218 (2019)
- [4] K.K. Deng, C.J. Wang, K.B. Nie, X.J. Wang, *Acta Metall. Sin. (Engl. Lett.)* **32**, 413 (2019)
- [5] S. Koleini, M.H. Idris, H. Jafari, *Mater. Des.* **33**, 20 (2012)
- [6] K. Song, F.S. Pan, X.H. Chen, Z.H. Zhang, A.T. Tang, J. She, Z.W. Yu, H.C. Pan, X.Y. Xu, *Mater. Lett.* **157**, 73 (2015)
- [7] M. Liu, P. Schmutz, P.J. Uggowitzer, G. Song, A. Atrens, *Corros. Sci.* **52**, 3687 (2010)
- [8] H. Miao, H. Huang, Y. Shi, H. Zhang, J. Pei, G. Yuan, *Corros. Sci.* **122**, 90 (2017)
- [9] K.B. Nie, K.K. Deng, X.J. Wang, F.J. Xu, K. Wu, M.Y. Zheng, *Mater. Sci. Eng. A* **624**, 157 (2015)
- [10] F. Lu, A. Ma, J. Jiang, Y. Guo, D. Yang, D. Song, J. Chen, *Corros. Sci.* **94**, 171 (2015)
- [11] P.P. Wu, F.J. Xu, K.K. Deng, F.Y. Han, Z.Z. Zhang, R. Gao, *Corros. Sci.* **127**, 280 (2017)
- [12] D. Sachdeva, *Corros. Sci.* **60**, 18 (2012)
- [13] M. Yamasaki, N. Hayashi, S. Izumi, Y. Kawamura, *Corros. Sci.* **49**, 255 (2007)
- [14] R. Arrabal, E. Matykina, F. Viejo, P. Skeldon, G.E. Thompson, *Corros. Sci.* **50**, 1744 (2008)
- [15] T. Zhang, G. Meng, Y. Shao, Z. Cui, F. Wang, *Corros. Sci.* **53**, 2934 (2011)
- [16] S.Z. Khalajabadi, M.R. Abdul Kadir, S. Izman, M. Kasiri-Asgarani, *Surf. Coat. Technol.* **277**, 30 (2015)
- [17] S.Z. Khalajabadi, A.B.H. Abu, N. Ahmad, M.A.M. Yajid, N.B. Hj Redzuan, R. Nasiri, W. Haider, I. Noshadi, *J. Mech. Behav. Biomed. Mater.* **77**, 360 (2018)
- [18] S.Z. Khalajabadi, M.A.M. Yajid, A.B. Haji Abu, N. Ahmad, N. Redzuan, A.F. Ismail, S. Asadi, I. Noshadi, *Mater. Chem. Phys.* **214**, 449 (2018)
- [19] R.H. Buzolin, M. Mohedano, C.L. Mendis, B. Mingo, D. Tolnai, C. Blawert, K.U. Kainer, H. Pinto, N. Hort, *Mater. Sci. Eng. A* **682**, 238 (2017)
- [20] X. Zhang, Y. Wu, Y. Xue, Z. Wang, L. Yang, *Mater. Lett.* **86**, 42 (2012)
- [21] Y. Song, D. Shan, R. Chen, E.H. Han, *Corros. Sci.* **52**, 1830 (2010)
- [22] J.S. Zhang, D. Wang, W.B. Zhang, H.X. Pei, Z.Y. You, C.X. Xu, W.L. Cheng, *Mater. Corros.* **66**, 542 (2015)
- [23] X. Zhang, Z. Ba, Z. Wang, Y. Xue, *Corros. Sci.* **105**, 68 (2016)
- [24] S.W. Xu, M.Y. Zheng, S. Kamado, K. Wu, G.J. Wang, X.Y. Lv, *Mater. Sci. Eng. A* **528**, 4055 (2011)
- [25] D.H. Bae, S.H. Kim, D.H. Kim, W.T. Kim, *Acta Mater.* **50**, 2343 (2002)
- [26] R.C. Zeng, W.C. Qi, H.Z. Cui, F. Zhang, S.Q. Li, E.H. Han, *Corros. Sci.* **96**, 23 (2015)
- [27] S.S. Li, B. Tang, D.B. Zeng, *J. Alloys Compd.* **437**, 317 (2007)
- [28] K. Hirai, H. Somekawa, Y. Takigawa, K. Higashi, *Mater. Sci. Eng. A* **403**, 276 (2005)
- [29] X. Gu, Y. Zheng, Y. Cheng, S. Zhong, T. Xi, *Biomaterials* **30**, 484 (2009)
- [30] F. Cao, Z. Shi, G.L. Song, M. Liu, M.S. Dargusch, A. Atrens, *Corros. Sci.* **90**, 176 (2015)
- [31] W.J. Li, K.K. Deng, X. Zhang, K.B. Nie, F.J. Xu, *Mater. Sci. Eng. A* **677**, 367 (2016)
- [32] M. Ascencio, M. Pegguleryuz, S. Omanovic, *Corros. Sci.* **87**, 489 (2014)
- [33] D. Song, A. Ma, J. Jiang, P. Lin, D. Yang, J. Fan, *Corros. Sci.* **52**, 481 (2010)
- [34] Z. Szklarz, M. Bisztyga, H. Krawiec, L. Lityńska-Dobrzyńska, Ł. Rogal, *Appl. Surf. Sci.* **405**, 529 (2017)
- [35] P. Minárik, R. Král, M. Janeček, *Appl. Surf. Sci.* **281**, 44 (2013)
- [36] Y. Song, D. Shan, E.H. Han, *J. Mater. Sci. Technol.* **33**, 954 (2017)
- [37] F.F. Cao, K.K. Deng, K.B. Nie, J.W. Kang, H.Y. Niu, *J. Alloys Compd.* **770**, 1208 (2019)
- [38] J.F. Wang, W.Y. Jiang, Y. Ma, Y. Li, S. Huang, *Mater. Chem. Phys.* **203**, 352 (2018)
- [39] J.W. Kang, C.J. Wang, K.K. Deng, K.B. Nie, Y. Bai, W.J. Li, *J. Alloys Compd.* **720**, 196 (2017)
- [40] H. Jia, X. Feng, Y. Yang, *J. Mater. Sci. Technol.* **34**, 1229 (2018)
- [41] J. Zhang, X. Niu, X. Qiu, K. Liu, C. Nan, D. Tang, J. Meng, *J. Alloys Compd.* **471**, 322 (2009)